Journal of Power Sources 267 (2014) 128–135

Contents lists available at ScienceDirect

Journal of Power Sources

journal homepage: www.elsevier.com/locate/jpowsour

Solid oxide-molten carbonate nano-composite fuel cells: Particle size effect

Shalima Shawuti [a], Mehmet A. Gulgun [a,b,*]

[a] Sabanci University, FENS, Orhanli Tuzla, Istanbul 34956, Turkey
[b] Sabanci University, SUNUM, Orhanli Tuzla, Istanbul 34956, Turkey

HIGHLIGHTS

- The amount of interface area influences conductivity of the composite strongly.
- In the composite electrolyte, the oxide surface acted as dissociating agent.
- The "liberated" ions at the interface around the oxide particles are more mobile.
- High mobility liberated ions give rise to high ionic conductivity.

ARTICLE INFO

Article history:
Received 2 January 2014
Received in revised form
18 April 2014
Accepted 3 May 2014
Available online 17 May 2014

Keywords:
Composite electrolyte
Ionic conductivity
Impedance spectroscopy
SOFC
Interphase
Activation energy

ABSTRACT

Varying the amount of specific interface area in the CeO_2–Na_2CO_3 nanocomposite fuel cell electrolyte helped reveal the role of interfaces in ionic conductivity. We mixed ceria particles with micrometer or nanometer size distributions to obtain a specific surface area (SSA) in the composite from 47 $m^2\ g^{-1}$ to 203 $m^2\ g^{-1}$. Microstructural investigations of the nanocomposite showed that the Na_2CO_3 phase serves as the glue in the microstructure, while thermal analysis revealed a glass transition-like behavior at 350 °C. High SSA enhanced the ionic conductivity significantly at temperatures below 400 °C. Moreover, the activation energy for the Arrhenius conductivity (σT) of the composites was lower than that of the Na_2CO_3 phase. This difference in the activation energies is consistent with the calculated dissociation energy of the carbonate phase. The strong dependence of conductivity on the SSA, along with differences in the activation energies, suggests that the oxide surface acted as a dissociation agent for the carbonate phase. A model for the solid composite electrolyte is proposed: in the nanocomposite electrolyte, the oxide surface helps Na_2CO_3 dissociate, so that the "liberated" ions can move easily in the interaction region around the oxide particles, giving rise to high ionic conductivities.

© 2014 Elsevier B.V. All rights reserved.

1. Introduction

Solid oxide fuel cells (SOFC), are regarded as an attractive alternative energy conversion system for electricity. However, a major drawback limiting a widespread commercialization of such systems was the high operating temperatures near 1000 °C of the current zirconia-based SOFC. Efforts to develop electrolyte and electrode materials based on doped ceria have been focused on reducing fuel cell operating temperature to an intermediate temperature range of 300–500 °C [1]. As such, ceria-based ceramics doped with various rare-earth elements are among the most promising candidates to become an intermediate temperature SOFC (IT-SOFC) electrolyte [2]. The ionic conductivity of doped ceria surpasses corresponding values of yttria-stabilized zirconia (YSZ) at the same temperature by up to 5–100 times [3]. However, an obstacle to the commercialization of ceria-based electrolytes is the reduction of ceria under an H_2 atmosphere. This reduction gives rise to electronic conductivity in the ionic conductor, thereby deteriorating the cell output voltage [4]. One solution proposed used a nano-composite electrolyte, composed of a carbonate and a ceria-based solid oxide [5–12]. In general, the so-called nano-composite electrolytes are composed of doped ceria particles embedded in alkali salts (carbonate, chloride, hydrate, or sulphate) [9,12,13]. The existing knowledge in the scientific literature presumes that oxide particles provide scaffolding for containing the

* Corresponding author. Sabanci University, FENS, Orhanli Tuzla, Istanbul 34956, Turkey. Tel.: +90 216 483 9536; fax: +90 216 483 9550.
E-mail addresses: shawuti@sabanciuniv.edu (S. Shawuti), m-gulgun@sabanciuniv.edu (M.A. Gulgun).

http://dx.doi.org/10.1016/j.jpowsour.2014.05.010
0378-7753/© 2014 Elsevier B.V. All rights reserved.

carbonate phase at the operating temperatures (400 °C–650 °C). Furthermore, it is assumed that such nano-composite electrolytes remain as two stable phases under the optimized operating conditions [13]. Impressively, this type of composite electrolyte has achieved a conductivity of 0.1 S cm^{-1} at 600 °C, attributed to the transport of H^+ ions and O^{2-} ions [13]. Because of these remarkable characteristics, one leading candidate electrolyte for a new generation of fuel cells is doped ceria nano-composites. Tang et al. investigated the morphological and electrical properties of composites with particle sizes varying from the micrometer to the nano-meter size scale. They found that nano-composite have significantly lower impedance values compared to the micron-sized composite [14]. In theoretical studies, Liu et al. have proposed that the interface layers between SDC and Na_2CO_3 matrix are the origin of the enhanced conductivity [15]. According to their findings, the interfaces would allow a "dual" conduction mechanism through the composite, via H^+ and O^{2-} transport. Furthermore, the pathways for H^+ ions were suggested to exist *along the interface between the component phases* [15]. The O^{2-} transport was assumed to occur through the interconnected SDC phase. According to theoretical calculations, conductivity of the composite electrolyte depended on the volume ratio of SDC to Na_2CO_3. Another study suggested that H^+ transport occurring along the "implied" interface dominated ionic conduction inside the electrolyte in the temperature range between 300 °C and 600 °C [16]. A conductivity of 0.1 S cm^{-1} was reported for a 20 wt% SDC-Na_2CO_3 nano-composite electrolyte at 300 °C [18]. This was the optimum carbonate amount in the composite according to Zhu et al. [18]. It was argued that conductivity resulted neither from the SDC nor from the Na_2CO_3 phase, as individual SDC and Na_2CO_3 phases are good electrical insulators at ~300 °C [17]. No other phase was detected in the composite. Hence the interface formed by the two phases was proposed to serve as a new conduction pathway for the nano-composite, offering on one hand a high-conductivity pathway for ionic conduction, and on the other hand, a presumed capacity to increase mobile ion concentration beyond that of the bulk [18]. No atomistic mechanisms have yet been suggested for either phenomenon.

Furthermore, Wang et al. claimed that the high conductivity of the nano-composite electrolyte was attributed to interfacial oxygen ion conduction rather than to bulk oxygen ion conduction [18]. The conduction through the interface was claimed to require low activation energy for O^{-2} transport. No explanation was given for the assumed low activation energy for the oxygen ion transport. The conductivity of the pure Na_2CO_3 is on the order of 10^{-5}–10^{-4} S cm^{-1} at the temperature range from 500 °C to 580 °C [15]. This value is much lower than the values reported for the nano-composite electrolyte in the literature [19]. However, in the literature for SDC – Na_2CO_3 nano-composite, the role of the Na_2CO_3 matrix was not discussed in detail.

An important role in the high ionic conductivity of the SDC – Na_2CO_3 nano-composite was attributed to the amorphous Na_2CO_3 [18]. It was further proposed that at rising temperatures, amorphous nature of Na_2CO_3 may reflect increased disorder of the Na_2CO_3 regions on the SDC surfaces. Therefore, Na_2CO_3 can better protect the surface of SDC and interfaces on a nano-scale and helps to facilitate oxygen ion transportation through the interfacial mechanism [19]. Similarly, for polymer-based composite electrolytes, ion mobility was larger in the amorphous regions, compared to the crystalline ones [20]. Therefore, the amorphous structure was more desirable for higher conductivity in the polymer electrolyte [21]. Composite electrolytes, in which nano-crystalline oxide particles were dispersed in an amorphous matrix, were the focus of attention in solid batteries and hybrid solar cells [22]. In such composite electrolytes, referred as "soggy sand", ion transport is mainly facilitated by amorphous regions of the soft matrix and not so much in crystalline parts. The ionic conductivity of amorphous regions was shown to be approximately 10^4 times higher than that of the crystalline phase [21,22].

The design and fabrication of a nano-composite electrolyte with a controlled total interface area between the SDC particles and the Na_2CO_3 matrix for a fixed mass ratio of components is thus the objective of this research paper. Tailoring an SSA enables the activation of the role of interfaces in the conductivity of composite electrolyte. The ionic conductivity and relaxation time of composite electrolyte were measured with electrochemical impedance spectroscopy (EIS). Our investigations were focused on the influence of total interface area between the ceramic particle and the alkali salt at a temperature range of 25 °C–600 °C.

2. Experimental procedure

Two types of samarium-doped ceria (SDC; $Sm_{0.2}Ce_{0.8}O_{1.9}$) powders (Fuel Cell Materials, Ohio, USA) with different particle sizes were used in the experiments. The nanometer-sized powder, referred to hereafter as N20, had primary particle sizes ranging from 5 nm to 10 nm. The micrometer-sized powder, referred to as HP, had a particle size distribution over 60 nm–150 nm. HP powders consisted of hard agglomerates made up of primary particles with 5–10 nm sizes. The measured specific surface areas (SSA) of N20 and HP powders were of 203 m^2 g^{-1} and 11 m^2 g^{-1}, respectively. Micrometer-sized SDC (HP) and nano-meter-sized SDC (N20) powders were mixed in the weight ratios of 4.35, 1.35, 0.92, 0.5, and 0.1 to form oxide powders with measured specific surface areas (SSA) of 47 m^2 g^{-1}, 93 m^2 g^{-1}, 110 m^2 g^{-1}, 140 m^2 g^{-1} and 185 m^2 g^{-1}. Afterwards, all oxide powders were combined with anhydrous Na_2CO_3 powder (Aldrich, Germany) to form a 10 wt% Na_2CO_3-SDC composite with specific interfacial area determined by the oxide powder SSA. The influence of the Na_2CO_3 amount in the composite will be discussed in an upcoming publication [23]. The weighed powder mixtures were dry-ball-milled for 6 h by using 3-millimeter diameter YSZ milling media in HDPE bottles. The milled powders were collected and re-ground by hand in an agate mortar and pestle before being uni-axially pressed into a pellet. Pellets made from the composite electrolyte were further subjected to isostatic compaction under 40 MPa in one step, to form a green compact with a diameter of 9 mm and a thickness of 1 mm. The pellets were heat-treated at 700 °C in air for 1 h. The heating rate was 5 °C min^{-1}.

The microstructure of the sintered composites was investigated using a scanning electron microscope (FEG-SEM Leo Supra 35, Oberkochen, Germany) equipped with an energy dispersive x-ray spectrometer (EDS, Roentec, Berlin, Germany). The thermal response of the powder mixtures and the sintered pellets in air was analyzed using a simultaneous thermal analysis system (NETZSCH STA-449C Jupiter, Selb, Germany). The measured water uptake of N20 and HP powders were revealed by TGA to be of 6% and 1%, respectively. The X-ray powder diffraction (XRD) patterns were recorded using a powder diffractometer (Bruker, Karlsruhe, Germany) with Cu Kα radiation (1.5418 Å) in the 2θ range of 10°–90°. A flash-dry silver paste (SPI Supplies, West Chester, USA) was used on both surfaces of the electrolyte pellet to provide electrical contact, covering the full top and bottom surfaces of the pellets. The complex resistivity of the pellets was measured by using a two-probe AC impedance spectrometer with an electrochemical interface (Solartron 1260 and 1286, respectively, Farnborough, UK), and an applied bias voltage amplitude of 100 mV AC. Electrochemical Impedance spectra (EIS) were recorded in the frequency range of 0.1 Hz–10 MHz from room temperature (RT) to 600 °C with a ProboStat™ cell (NorECs, Oslo, Norway) under air atmosphere. A

parallel RC equivalent circuit was fitted to high frequency and low frequency data with the Z-View program (Scribner AI, Southern Pines, NC, USA). The total area of the silver electrodes was used in the conductivity calculation. High frequency resistance and high frequency capacitance were obtained from the fitted first semi-circle, as described in the relevant literature [24]. Similarly, the low frequency data were obtained by employing same procedure. The relaxation times (τ) were also calculated by using the relationship, $\tau = CR$, where C is the capacitance, R is the resistivity [25].

3. Results

The phase distribution and possible reactions between the constituent phases of composite were investigated by using XRD. Fig. 1 shows the XRD patterns obtained from as-received SDC (HP) powders and composite prepared with SDC (HP) and Na_2CO_3 powders after a heat-treatment of 700 °C for 1 h. The composites contained 10 wt% of Na_2CO_3 powders. In Fig. 1, all the diffraction peaks detected in XRD patterns of composite were originating from SDC crystal planes. Each peak could be identified with the SDC plane indices, i.e. (110), (200), (220), (311), (222), (400), (331) and (420). No diffraction peaks belonging to crystalline Na_2CO_3 could be observed in the XRD spectrum of the nano-composite. The XRD spectra from as-received crystalline Na_2CO_3 and Na_2CO_3 powders after heat-treatment (700 °C for 1 h) are shown in Fig. 1 inset. The XRD spectrum from as-received powders revealed diffraction peaks from monosodium carbonate ($NaHCO_3$) which are marked in the inset, alongside the peaks of the Na_2CO_3 phase. Apparently, the Na_2CO_3 phase reacted with the atmospheric moisture to form some monosodium carbonate in the as-received powders. During the heat-treatment process, the hydrated, as-received Na_2CO_3 lost its monohydrate water, as can be seen from the disappearance of the monosodium carbonate peaks at 2θ values of 32°, 34° and 36° in Fig. 1 inset.

Fig. 2 shows an image of the composite containing 10 wt% Na_2CO_3 prepared with micrometer size SDC (HP) oxide particles, as viewed in cross-section in the scanning electron microscope. The lower atomic number Na_2CO_3 matrix phase (transparent dark contrast) and the higher atomic number SDC particles (bright particles) are delineated with circles. The image reveals that Na_2CO_3 covered the SDC particle surfaces uniformly and constituted the matrix phase in the composite microstructure. The high average atomic number of the ceria particles facilitated identification of individual oxide particles in the composite electrolyte samples, as circled in Fig. 2. The cross-section SEM image also showed that the average grain size in SDC (HP) composite pellet is smaller than 1 μm and the relative density to be ≥98%. Na_2CO_3 appears to have served as the glue for the oxide particles. In the microstructure, both component phases appear to be interconnected in 3 dimensions. One can still recognize the edges of the prismatic shapes of the oxide particles. No indication of dissolution was observed for oxide particles within the Na_2CO_3 matrix, nor of reaction products between the two components at these heat-treatment temperatures (at 700 °C for 1 h).

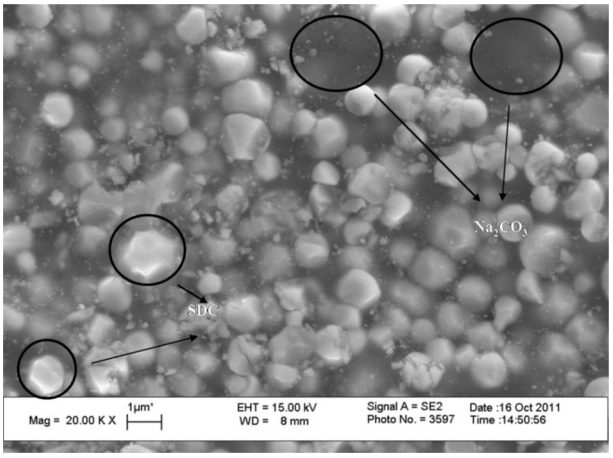

Fig. 2. The Cross sectional-SEM images of the composites that were made of SDC (HP). Composite contained 10 wt% Na_2CO_3 matrix phase and heat-treated at 700 °C for 1 h.

The thermal response of the individual constituent phases and the sintered composite pellet were analyzed using a simultaneous thermal analysis (DTA/TGA and DSC) system. As shown in Fig. 3, the DTA thermograph of the SDC (N20) Na_2CO_3 10 wt% composite pellet was compared with that of a heat-treated Na_2CO_3 pellet. The DTA spectrum of the SDC (N20)-Na_2CO_3 10 wt% composite pellet revealed a small endothermic peak at the temperature ~840 °C, which corresponds to the melting temperature of Na_2CO_3. This

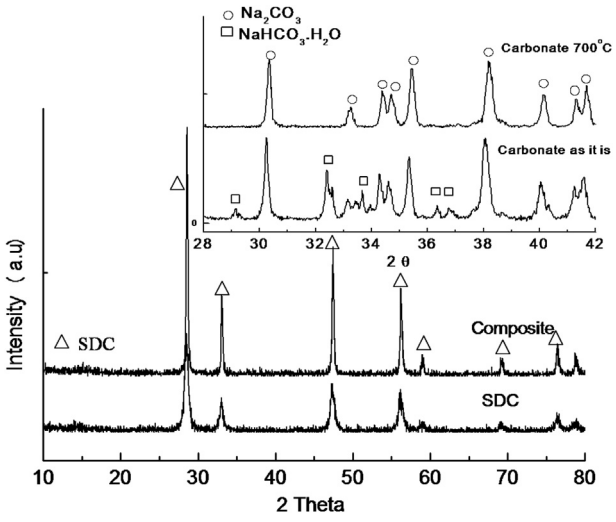

Fig. 1. The room temperature XRD patterns of the SDC (HP) and the milled composite powder from SDC (HP) - Na_2CO_3 10 wt%. Inset: The room temperature XRD patterns of the Na_2CO_3 as received and after the heat-treatment at 700 °C for 1 h. The peaks belonging to monosodium carbonate ($NaHCO_3$) are marked, alongside the peaks of the Na_2CO_3 phase in the inset.

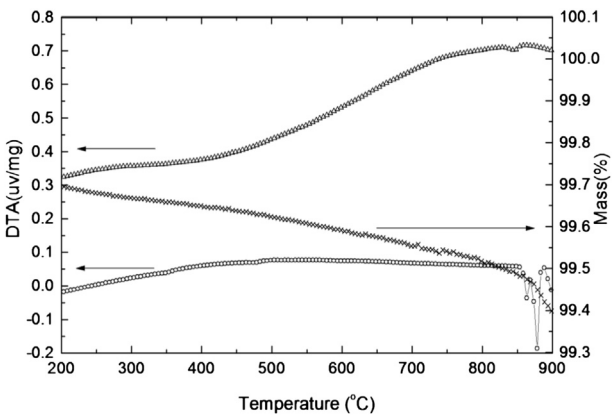

Fig. 3. The DTA spectra of the SDC (N20) Na_2CO_3 10 wt% (represented as up triangle) and Na_2CO_3 (represented as a circle). The composite pellet and Na_2CO_3 pellet were heat-treated at 700 °C for 1 h. The TGA plot of the Na_2CO_3 after the heat-treatment at 700 °C for 1 h is represented by connected cross line.

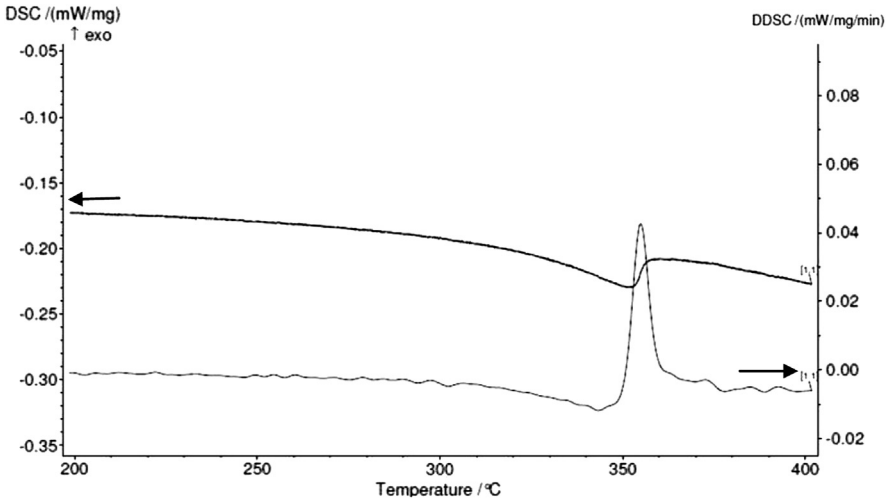

Fig. 4. The DSC curve and its derivative for the as-received Na_2CO_3 powder.

temperature is also the temperature at which decomposition of Na_2CO_3 started. The TGA curve of the heat-treated Na_2CO_3 pellet also indicated the melting and consequent decomposition of the Na_2CO_3 over the same temperature range (shown as a connected cross line in Fig. 3). Fig. 4 shows the results of DSC analysis of the as-received Na_2CO_3 powder. The step change in the baseline of the DSC response, corresponding to change in the heat capacity, is typical of a glass-transition type of structural relaxation in an amorphous material. Therefore, it could be indicative of a glass transition-like softening process in the amorphous Na_2CO_3 matrix.

The electrical response of the samples was studied by using an impedance analyzer. Temperature dependence of the complex resistivity was displayed in a Nyquist type-plot. Nyquist-type plots display the relationship between the real part of the complex resistance (Z′) and the negative imaginary part of resistance (−Z″). The complex curve format is an essential and convenient tool to distinguish the ac conductivity and relaxation times in the bulk versus grain boundary regions. It facilitates a quick insight into the electrical processes typically characterized by the smallest capacitance of the material [25]. The smallest semi-circle corresponds to the highest capacitance in the Nyquist plot (i.e., Z′ vs −Z″). In a single phase polycrystalline ceramic, the semi-circular features in Nyquist-type plots are generally interpreted as being the impedance responses of the bulk, the grain boundary and the electrode polarization, towards decreasing frequency [25]. Fig. 5 shows two sets of representative Nyquist-type plots and imaginary impedance

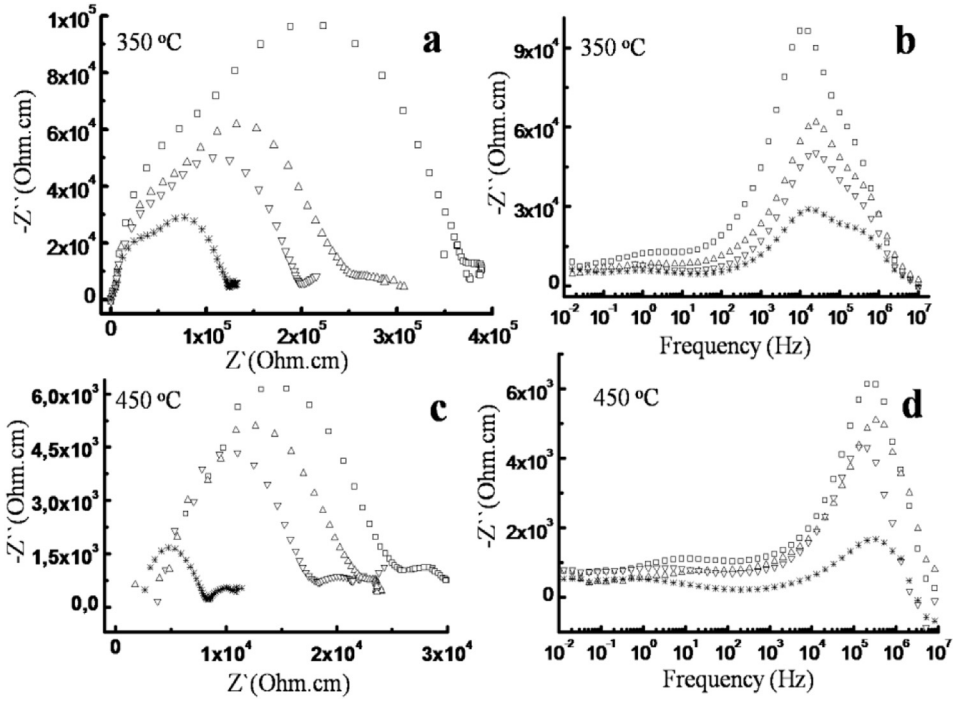

Fig. 5. Nyquist spectra and imaginary impedance (−Z′) versus frequency plot of the 10 wt% of Na_2CO_3 composites with different SSA of SDC powders. All measurements were taken in air atmosphere at temperatures between 350 °C and 450 °C. Composite pellets were sintered at 700 °C for 1 h (square 47 $m^2\ g^{-1}$, up-triangle 110 $m^2\ g^{-1}$, down-triangle 140 $m^2\ g^{-1}$, star 203 $m^2\ g^{-1}$).

versus frequency plots measured at 350 °C and 450 °C. In this study, features in the Nyquist plots obtained from the nano-composite electrolytes were labeled simply as a low-frequency or high-frequency arc without assigning them to any specific micro-structural feature. In the nano-composite, it should be noted that there are at least two chemically distinct components, even without assuming any interfaces or grain boundaries within or in between them. The values reported for the conductivity (S cm^{-1}) were derived from the intercepts of the semi-circular arcs in the Nyquist-type plots. At relatively high temperatures, such as 350 °C, the electrode polarization effect appeared at the very low frequency region of the spectra [26] in Fig. 5. In the plots, low amplitude broad arcs at frequencies below 10 Hz confirm the electrode polarization in this frequency range [26] (see Fig. 5b and d). This low frequency tail was a strong evidence for the ionic-only character of the electrical conduction the nano-composite material [27]. At all measured temperatures, as the SSA of the composites increased impedance curves were reduced in amplitude, indicating an increase in the conductance of the samples. Further analysis of the individual arcs in the impedance curves revealed that with increasing SSA, the ratio of the size of the low frequency arc to the size of the high frequency arc varied randomly; and no trend could be established.

Relaxation time constants (τ) were calculated by applying the Z-View algorithm for fitting semicircular arcs to the low-frequency and high-frequency arcs. The corresponding τ values are listed in Table 1. Within the measured frequency range, relaxation times of the high-frequency phenomena were different for all composites at 350 °C. In contrast, relaxation times for the low frequency arcs were consistent within experimental error limits. The relaxation time constants of the constituent matrix phase (Na_2CO_3) and the particulate phase (SDC HP) for the same temperature (350 °C) were also calculated for comparison.

Fig. 6 summarizes the variation in total ionic conductivity of the nano-composites prepared from SDC particles with different SSA as function of temperature. At low temperatures, the ionic conductivities of the composites with smaller SSA were lower than that of the composites with larger SSA. Conductivities increased monotonically with increasing SSA of SDC particles in the composite at all measured temperature ranges. At lower temperatures, the amount of interface area (SSA of SDC particles) had a stronger influence on the ionic conductivity than at temperatures above 400 °C. The composite with the highest SSA SDC powders had the highest total ionic conductivity. With increasing temperature, the influence of SSA on conductivity became weaker.

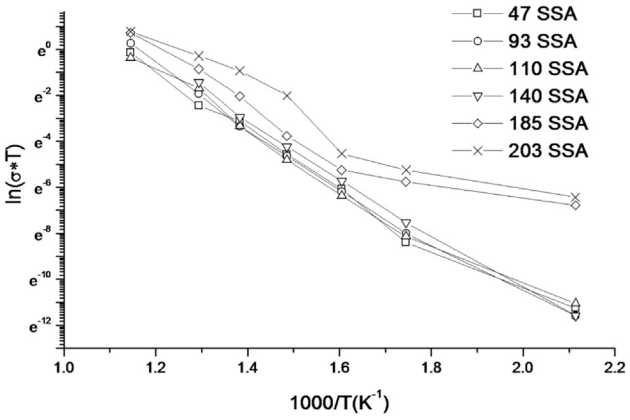

Fig. 6. The conductivity of the composite SDC-Na_2CO_3 10 wt% as a function of SSA from 200 °C to 550 °C. (square 47 m^2 g^{-1},circle 93 m^2 g^{-1}, up-triangle 110 m^2 g^{-1}, down-triangle 140 m^2 g^{-1}, diamond 185 m^2 g^{-1}, cross is composite with SDC N20).

4. Discussion

4.1. Phase distribution in the composite

Micro-structural analysis of the composites has shown that the processing steps were successful in generating a dense and uniform nano-composite electrolyte. Although Na_2CO_3 was only 10 wt% of the composite (corresponding to 23 vol%), it constituted the matrix phase and glued the oxide nano-particles together during the 1 h heat-treatment at 700 °C. Compacts prepared with SDC powders and heat-treated under the same conditions (at 700 °C for 1 h), disintegrated easily upon application of a slight stress, indicating that the SDC compacts could not be sintered sufficiently. XRD investigations of sintered composite pellets showed that no additional new phases had formed. In fact, the composite XRD peaks in Fig. 1 only belonged to the crystalline peaks of SDC. The XRD quantification showed that as-received carbonate powders contained of Na_2CO_3, $NaHCO_3$. $Na_2CO_3.H_2O$, and $Na_2CO_3.2H_2O$. During the heat treatment, hydrated carbonate phases decomposed. Firstly, $NaHCO_3.Na_2CO_3$. H_2O and $Na_2CO_3.2H_2O$ lost their water molecules. Secondly, $NaHCO_3$ decomposed at 160 °C to Na_2CO_3. No distinguishable peak could be assigned to the Na_2CO_3 phase in the XRD spectrum of the composite. This is partly due to the structure factor differences (which are in this case related to the atomic number (Z of the element) making up the compounds) between the SDC and the carbonate phase. SDC is primarily made up of heavy cations like Sm ($Z = 62$) and Ce ($Z = 58$) besides oxygen, while the average Z of Na_2CO_3 is only 14 [28]. The other reason why no crystalline peaks belonging to carbonate phase was observed may be attributed to the fact that at least a large portion of the Na_2CO_3 phase in the composite was amorphous. The XRD results combined with the SEM microstructure shown in Fig. 2, confirmed that a large portion of the carbonate matrix phase was in an amorphous form and that there were no chemical reactions leading to the formation of a new compound between the oxide phase SDC and the Na_2CO_3.

Thermal analysis and X-ray diffraction analysis revealed also that during the heat-treatment at 700 °C, the hydrated portion of the as-received Na_2CO_3 phase lost its monohydrate water (see Fig. 1 inset). Additionally, thermal analysis of the nano-composite revealed a small but distinguishable endothermic peak at 840 °C without an associated weight loss. This feature was assigned to melting of the crystalline portion of the Na_2CO_3 phase. On the other hand, the DSC and dilatometer thermograms of the composite, as well as ball milled Na_2CO_3 powder, revealed a glass transition occurring at a temperature around 350 °C (see Fig. 4). From these experimental results, it can be concluded that a large portion of the

Table 1
The calculated relaxation time constant of the SDC (HP pellet), Na_2CO_3 pellet and composite SDC-Na_2CO_3 10 wt% as a function of SSA at 350 °C. (47 m^2 g^{-1}, 93 m^2 g^{-1}, 110 m^2 g^{-1}, 140 m^2 g^{-1}, 185 m^2 g^{-1}, 203 m^2 g^{-1}).

	47 ssa	93 ssa	110 ssa	140 ssa	185 ssa	203 ssa	SDC	Na_2CO_3
High frequency (Hz)	9.80E-07	3.20E-06	6.40E-06	3.80E-06	1.80E-06	1.40E-06	4.00E-07	4.90E-08
Low frequency (Hz)	6.10E-06	8.80E-06	4.60E-06	9.90E-06	5.20E-06	7.00E-06	7.90E-07	1.90E-07

Na_2CO_3 matrix phase was in an amorphous state with some crystalline Na_2CO_3 still present in the composite structure. Other studies in the literature also reported an amorphous Na_2CO_3 phase, which was presumed to have formed after the heat-treatment of SDC and Na_2CO_3 composite [29].

4.2. Ionic conductivity: temperature dependence of mechanisms

Ionic conductivity behavior and other electrical properties of the electrolyte nano-composite were determined by impedance analysis. The impedance analyses of composites with different SSA (*i.e.*, interface area) revealed the influence of the amount of oxide surface on conductivity. Total resistivity decreased with rising temperature, indicating a negative temperature coefficient of resistance (NTCR) of the composites [30]. With increasing SSA, *i.e.*, smaller sized oxide particles, both ($-Z''$) and (Z') values decreased and conductivities increased monotonically at all measurement temperatures (Fig. 6). The resistivity values of the composite with a high SSA, *i.e.*, ~203 $m^2\ g^{-1}$, was on the order of 1.2×10^5 Ω-cm, while the one for the composite with a lower SSA, 47 $m^2\ g^{-1}$, was around 3.8×10^5 Ω-cm at 350 °C. This resistivity was 3 times higher in magnitude than the resistivity of the composite with larger (203 $m^2\ g^{-1}$) surface area. At room temperature, due to the very high resistivity values of the composite, it was difficult to fit the experimental data in the Nyquist plots to semicircles. A depressed semi-circular shape for the arcs of Nyquist plots was observed in EIS spectra for all composites. All Nyquist plots of the composites with different SSA exhibited two overlapping semi-circular arcs at 350 °C. The Nyquist plots for the composite were significantly different from the one of a single phase electrolyte material, such as LSGM, which usually exhibits only a single semi-circular arc in the complex impedance curve [24]. These overlapping semi-circular arcs were a consequence of at least two coexisting conduction events with different relaxation times [24,26,28–30]. The imaginary impedance versus frequency spectra of the composite electrolytes, measured at the temperature of 350 °C, is presented in Fig. 5b. The observation of the two maxima in the curves may be associated with a distribution of relaxation times at the complex resistivity level (representative of a dispersive behavior of the impedance). If there would be no dispersion, the curve would be reduced to that of a single time-constant behavior [26].

The measured τ-values for the composite do not correspond to the τ-values calculated for SDC or Na_2CO_3 phases. They were consistently smaller than the τ—values of either constituent phase. In addition, it was observed that the SSA of the oxide powders had a strong influence on the resistivity of the composite. The higher the amount of interface between the oxide powder and the Na_2CO_3 matrix, the higher was the ionic conductivity. Shorter time constants also suggested that the mobile species in the composite were faster and could respond to higher frequencies. The synergistic interaction of the matrix phase and the oxide surface in the composite apparently generated a new path, along which mobile ions can move faster and/or with greater ease. Therefore, it is reasonable to suggest that the two or more relaxation time constants are due to the additional conduction path stemming from the interfaces within the composites. Those highly mobile ions in the regions near interface were expected to follow the AC field up to higher frequency, causing a shift of the peak maxima towards higher frequencies in Fig. 5b and d. This shift has led to shorter relaxation times [31].

At temperatures above 450 °C, the complex impedance response (Nyquist plots) of all composite revealed only one dominant semicircular arc. For all measured temperature ranges, the so-called Arrhenius conductivity (σT) of the composites with higher SSA was larger than the conductivity of the composites with lower SSA (shown in Fig. 6). The temperature around 350 °C is the temperature range in which both the composite and ball milled Na_2CO_3 showed a glass transition-like thermal behavior (Fig. 4). It is believed that above 350 °C, Na_2CO_3, *i.e.*, the matrix phase, takes a dominating role in the conductivity due to its softened amorphous structure. Therefore, above this temperature there is only a single semicircle visible in the impedance curves due to conduction primarily dominated by the matrix phase. Below 350 °C, *i.e.* below the softening of the matrix phase, SSA played the major role. The ionic conductivity of the SDC – Na_2CO_3 with the highest SSA (203 $m^2\ g^{-1}$) is 3 times larger in magnitude than the conductivity of composite with the SSA (47 $m^2\ g^{-1}$) in this temperature range. All of the composites have exactly the same weight ratio of the Na_2CO_3 phase to the oxide phase in their corresponding composition. Therefore, the only difference was the oxide particle size and the amount of SSA of the oxide particles, which are related to each other as SSA ~[1/particle size]. When conductivities of the SDC pellets prepared with nano-sized or micrometer-sized ceria particles were compared, there was not a significant difference in their values. Therefore, the observed effect can be attributed to the interaction of the oxide surface with the Na_2CO_3 phase.

The high conductivity measured in the composite with the highest surface area may stem from the interplay between two phenomena: The first phenomenon is related to the hygroscopic nature of the Na_2CO_3. In the conductivity plots of the composites (see in Fig. 6), at temperatures around 200 °C, conductivity values for the highest SSA at constant amount of carbonate, was several times higher than the sample with lowest SSA. At higher temperatures, after 350 °C, the amount of interface area played a lesser role unlike it did below this temperature. One of the reasons for the difference in the low temperature (*i.e.*, ≤200 °C) conductivity might be due to the difference in the water uptake of different SDC powders with dramatically different SSA's. Since SDC nano-powders with 203 $m^2\ g^{-1}$ SSA will absorb 5% more water per gram from environment than the SDC micro-powders with 47 $m^2\ g^{-1}$ SSA they have a higher propensity to form hydrated carbonate phase (i.e. $NaHCO_3$) during mechanical mixing. Therefore, the hygroscopic nature of the composite is a key for the enhanced conductivity performance at low temperatures, *i.e.*, $T \leq 200$ °C. As the same sample conductivity was measured for a second time, after it has been exposed to temperatures above 350 °C, the superior performance of nano-powders with 203 $m^2\ g^{-1}$ SSA below 200 °C was not observed. This can be attributed to the decomposition of $NaHCO_3$ to Na_2CO_3 phase above temperature ~150 °C. Fig. 7 shows a simplified sketch of the composite material consisting of nano-crystalline SDC particles (large circle) and a second phase (a mixture of Na_2CO_3 and $NaHCO_3$). The second effect on the conductivity may stem from the interaction of the oxide surface with the matrix phases. The interfaces in the composite electrolyte were suggested to include regions between the ionic conductor SDC grains and the Na_2CO_3 phase [2,4,15,17]. Those regions were supposed to lead to positive effects in the conductivity of composite materials at lower temperature. In a different electrolyte-oxide particle composite system, Liang discovered that for the composite LiI:Al_2O_3, when the insulator Al_2O_3 were added to the Li ion conductor LiI, the overall conductivity of the material increase [24]. This unexpected improvement from an insulating oxide was explained by an enhanced conductivity in the interfacial regions that form between the charged oxide particle surfaces and the electrolyte phase. Such systems were termed "dispersed ionic conductors" or better known as "soggy sand" [32]. Conventionally, these have been composites of liquid (electrolyte) matrix phase and dispersed sub-micrometer insulator particles. With the addition of oxide particles, the composite showed significant improvement in the

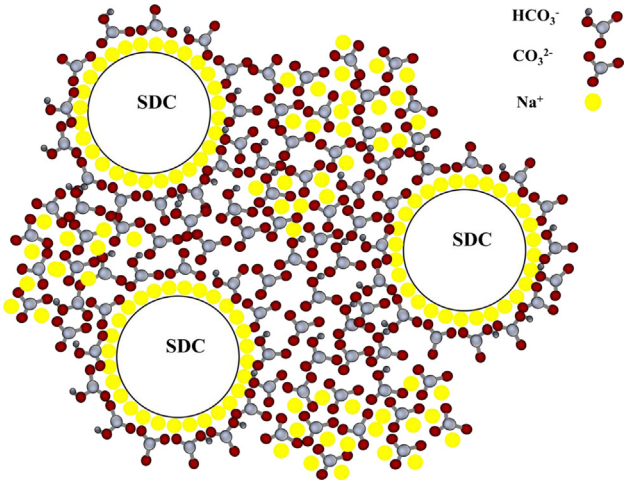

Fig. 7. The schematic illustration of composite electrolyte materials of SDC and Na_2CO_3.$NaHCO_3$. A network of conduction paths consists of interfaces between oxygen ion conductor SDC grains and Na_2CO_3/$NaHCO_3$ phase.

ionic conductivity. There were several attempts to explain this unexpected behavior. The suggestions included formation of space charge layers, an enhanced concentration of dislocations, or the formation of new phases [33,34]. The one model gaining widespread acceptance is the "soggy sand," model, in which the oxide surface attracts one type of ionic species from the liquid electrolyte, so that the other ionic species are accommodated in the region surrounding the oxide particles, where they form a "superionic" interphase [13]. The presence of such highly conducting interphase (which were wrongly termed interfaces in the existing literature) lead to a pronounced increase in the total ionic conductivity. Our and other experiments reported in the literature with varying volume of oxide particles showed a percolation type of behavior, strengthening the idea of conducting interphase around the particles.

In the composite electrolyte investigated in this study, the strongest influence on conductivity was observed to be from the amount of interface area and the temperature. As the composite softened above the temperature range of 350 °C, the conductivity became less dependent on the change in the interface area. Conductivity plots of all composites followed a trend very similar each other. The slope of the conductivity plot of the composite electrolyte exhibited two distinct values above and below 350 °C. The smaller activation energy observed at low temperatures (below 350 °C) is attributed to contributions from Na_2CO_3, as well as $NaHCO_3$, to the ionic conductivity in composite electrolyte. Above 200 °C, an conduction from $NaHCO_3$ was not expected as $NaHCO_3$ decompose ~150 °C. The activation energy of the composite calculated from such plots differs from the activation energy for pure Na_2CO_3 or pure SDC samples. For Na_2CO_3 and the composite, the calculated activation energies were around 2.3 ev and 1.5 ev, respectively. The difference in the activation energies for conduction between composite and pure Na_2CO_3 was very close to the dissociation energy for the carbonate phase estimated by Rajaskhar et al. [35]. In "soggy sand" model for liquid electrolytes in Li-ion batteries, it was suggested that the oxide surface serves as a dissociation agent for the molecule. The measured activation energies in these solid composite electrolyte indicated that a similar function could be fulfilled by the SDC particles in the nanocomposite. The dependence of ionic conductivity on the SSA and the type of oxide surface strengthened this interpretation. The influence of different oxide surfaces on the conductivity of the composite is the subject of an upcoming publication [23]. In light of such observations, a model for the solid composite electrolyte was proposed that is illustrated in Fig. 7. The model suggested that in ceria based nano-composite electrolyte, the function of the SDC surface is to help Na_2CO_3 (and $NaHCO_3$) to dissociate, *i.e.* split into Na+, (and/or H+) and CO_3^{2-} ion complexes. Then, one type of ions, depending on the surface-charge of the oxide particle, is adsorbed on the oxide surface. The counter, i.e. "liberated" ions can now move more easily in the interphase region around the oxide particles. Thus, the activation energy for ionic conduction in the composite is lower than the activation energy of the pure matrix phase, *i.e.* Na_2CO_3. In the proposed model, the SDC oxide surface helps Na_2CO_3 to dissociate so that Na^+ (and/or H^+) will adsorb to the surface. This leaves the CO_3^{2-} ion in regions around the particles. At a certain oxide particle volume ratio those regions overlap to give a conductive ion-path. This model helps explain the effect of amount of surface area and the observed behavior of the ionic conductivity as a function of amount and size of oxide particles in the composite electrolyte. According to this model above the softening point of the matrix carbonate phase as the conduction within the bulk of the matrix phase would be also getting easier the influence of the different surface areas should get less. This is exactly the behavior observed in the composite above 350 °C where both Na_2CO_3 and the composite showed a glass transition like behavior. Further impedance and electron microscopy studies with solid composite electrolytes are underway to shed more light on to the conduction mechanisms that may be operative in nanocomposite electrolytes based on oxide nanoparticles embedded into solid salt matrices.

5. Conclusion

We presented an approach of designing and developing controlled amount of interface area in the SDC-Na_2CO_3 composite electrolyte. Varying the amount of specific interface area between constituent phases in the nano-composite electrolyte provided insight into the role of interfaces in the ionic conductivity. For all the SDC – Na_2CO_3 nano-composite with different SSA, a uniform and homogeneously dispersed microstructure was fabricated. Micro-structural investigations by SEM indicated that the Na_2CO_3 phase served as the glue and was at least partially amorphous. The virgin nano-composite electrolyte contained $NaHCO_3$ alongside SDC and Na_2CO_3. The $NaHCO_3$ decomposed when heated above 150 °C.

At lower temperatures (*i.e.*, ≤400 °C), the amount of SSA plays a determining role in the ionic conductivity. A glass-transition-like behavior was observed of the nano-composite at 350 °C. Above this temperature, the effect of SSA tended to diminish and the softened Na_2CO_3 matrix phase began to dominate the ionic conductivity. Activation energies for the Arrhenius conductivity (σT) of the composites calculated for the 25 °C–600 °C range were lower than that of the Na_2CO_3 matrix phase by an amount that was similar to the calculated dissociation energy of the carbonate phase in the literature. The strong dependence of the conductivity on the SSA, alongside the calculated activation energies, suggested that the oxide surface acted as a dissociation agent for the carbonate phases. Depending on the charge of the oxide particle surface, one type of ions was adsorbed on the particle surface. The other "liberated" ion could move easier in the interphase region around the oxide particles. In light of such observations, a model for the solid composite electrolyte was proposed. In this model, the highly conducting interconnected interphases containing the "liberated" ions lead to a pronounced increase in the total ionic conductivity.

Acknowledgment

The authors would like to gratefully acknowledge the graduate project supports by the TUBITAK, Turkey. We would like to acknowledge the Junior Travel supports by the I2CAM-NSF Grant Number DMR-0844115. We also would like to acknowledge the Yamanashi University, Green Energy for the travel support and The research leading to these results has received funding from the European Union Seventh Framework Programme under Grant Agreement 312483 - ESTEEM2 (IntegratedInfrastructureInitiative–I3) via project number *20121206-GULGUN*. We would like to acknowledge very valuable discussions on the manuscript with Dr. C. Ow-Yang.

References

[1] Ç. Öncel, B. Özkaya, M. Gülgün, J. Eur. Ceram. Soc. 27 (2007) 599.
[2] H. Jianbing, M. Zongqiang, L. Zhixing, W. Cheng, J. Power Sources 175 (2008) 238.
[3] Q.X. Fu, G.Y. Meng, B. Zhu, J. Power Sources 104 (2002) 73.
[4] Martín G. Bellino, Diego G. Lamas, Noemí E. Walsöe de Reca, J. Mater. Chem. 18 (2008) 4537.
[5] B. Zhu, J. Power Sources 114 (2003) 1.
[6] B. Zhu, J. Power Sources 93 (2001) 82.
[7] W. Zhu, C. Xia, D. Ding, X. Shi, G. Meng, Mater. Res. Bull. 41 (2006) 2057.
[8] B. Zhu, X. Liu, M. Sun, S. Ji, J. Sun, Solid State Sci. 5 (2003) 1127.
[9] L. Xue, X. Guoliang, K. Huang, J. Electrochem. Soc. 158 (2011) 225.
[10] B. Zhu, X. Liu, P. Zhou, X. Yang, Z. Zhu, W. Zhu, J. Electrochem. Commun. 3 (2001) 566.
[11] B. Zhu, Solid State Ionics 145 (2001) 371.
[12] G. Abbas, R. Raza, M. Ashraf Ch, B. Zhu, J. Fuel Cell Sci. Technol. Res. Pap. 8 (2011) 041013.
[13] B. Zhu, Mahmut D. Mat, Int. J. Electrochem. Sci. 1 (2006) 383.
[14] Z. Tang, Q. Lin, B. Mellander, B. Zhu, Int. J. Hydrogen Energy 35 (2010) 2970.
[15] L. Qinghua, B. Zhu, Appl. Phys. Lett. 97 (2010) 183115.
[16] W. Xiaodi, M. Ying, R. Raza, M. Muhammed, B. Zhu, Electrochem. Commun. 10 (2008) 1617.
[17] B. Zhu, X.T. Yang, J. Xu, Z.G. Zhu, S.J. Ji, M.T. Sun, J.C. Sun, J. Power Sources 118 (2003) 47.
[18] Xiaodi Wang, PhD Thesis, KTH University, Sweden, 2010.
[19] Y. Liu, B. Li, X. Wei, W. Pan, J. Am. Ceram. Soc. 12 (2008) 3926.
[20] B. Kumar, S.J. Rodrigues, Solid State Ionics 167 (2004) 91.
[21] K. Das Shyamal, A.J. Bhattacharyya, J. Phys. Chem. 113 (2009) 6699.
[22] A.J. Bhattacharyya, Jürgen Fleig, Yu-Guo Guo, Joachim Maier, Adv. Mater. 17 (2005) 2630.
[23] S. Shawuti, PhD Thesis, Sabanci University, Turkey, 2013.
[24] E.J. Abram, D.C. Sinclair, A.R. West, J. Electroceram. 7 (3) (2001) 179.
[25] E. Barsoukov, J. Ross Macdonald, second ed., John Wiley & Sons, New Jersy, 2005, 252.
[26] D. Pergolesi, E. Fabbri, A. D'Epifanio, E. Di Bartolomeo, A. Tebano, S. Sanna, S. Licoccia, G. Balestrino, E. Traversa, Nat. Mater. 9 (2010) 846.
[27] C.M. Lapa, F.M.L. Figuiredo, D.P.F. de Souza, L. Song, B. Zhu, F.M.B. Marques, Int. J. Hydrogen Energy 35 (2010) 2953.
[28] W. Yaseda, K. Suzuki, Z. Phys. B 20 (1975) 3433.
[29] Y. Ma, X. Wang, R. Raza, M. Muhammed, B. Zhu, Int. J. Hydrogen Energy 35 (2010) 2580.
[30] Lily, K. Kumari, K. Prasad, R. Choudhary, J. Alloys Compd. 453 (2008) 325.
[31] C.C. Liang, J. Electrochem. Soc. 120 (1973) 1289.
[32] P. Heitjans, S. Indris, J. Phys. Condens. Matter 15 (2003) 1257.
[33] J. Maier, Ber. Bunsenges. Phys. Chem. 88 (1984) 1057.
[34] N.J. Dudney, Annu. Rev. Mater. Sci. 19 (1989) 113.
[35] B. Rajaskhar, J.M.C. Plane, Geophys. Res. Lett. 20 (1993) 21.